

Terrestrial Effects of Nearby Supernovae: Updated Modeling

Brian C. Thomas¹ and Alexander M. Yelland^{1,2}

1. Department of Physics and Astronomy, Washburn University, Topeka, Kansas 66621 USA, brian.thomas@washburn.edu
2. Department of Physics, Massachusetts Institute of Technology, Cambridge, MA 02139

ABSTRACT

We have re-evaluated recent studies of effects on Earth by cosmic rays (CRs) from nearby supernovae (SNe) at 100 pc and 50 pc, in the diffusive transport CR case, here including an early time suppression at lower CR energies neglected in the previous work. Inclusion of this suppression leads to lower overall CR flux at early times, lower atmospheric ionization, smaller resulting ozone depletion, and lower sea-level muon radiation dose. Differences in atmospheric impacts are most pronounced for the 100 pc case with less significant differences in the 50 pc case. We find a greater discrepancy in the modeled sea-level muon radiation dose, with significantly smaller dose values in the 50 pc case; our results indicate it is unlikely that muon radiation is a significant threat to the biosphere for SNe beyond at least 20 pc. We have also performed new modeling of effects by SNe at 20 pc and 10 pc. Overall, our results indicate that, considering only effects of SN CRs, the “lethal” SN distance may be closer to 20 pc rather than the typically quoted 8-10 pc.

Key words: supernovae, ozone, extinctions

1 INTRODUCTION

In recent years, multiple discoveries of live ^{60}Fe on Earth (Knie et al. 2004; Ludwig et al. 2016; Wallner et al. 2016, 2020), the Moon (Fimiani et al. 2016), and in near-Earth space (Binns et al. 2016) has established the occurrence of at least one, and most likely several, core-collapse supernovae (SNe) within 50-100 pc from Earth (Breitschwerdt et al. 2016; Fry et al. 2016) around 2.6 million years ago. Possible effects on Earth's atmosphere, biosphere, and climate by such supernovae have been investigated (Melott et al. 2017, 2020, 2019; Melott & Thomas 2019; Thomas 2018; Thomas et al. 2016; Thomas & Ratterman 2020). Predicted effects include depletion of stratospheric ozone with subsequent surface-level increase in solar ultraviolet radiation; increased muon and neutron radiation exposure at Earth's surface and into oceans; a possible increase in wildfires following increased lightning rates; and minor climate changes due to changes in atmospheric ozone profiles.

Each of these recent studies relies on modeling of the flux at Earth of cosmic ray protons accelerated by the nearby supernovae (hereafter, SNCR). For certain cases in previous work diffusive transport of CRs was assumed; however, calculations reported therein (Melott et al. 2017; Thomas et al. 2016) neglected to include a factor in the diffusive transport equation that results in a suppression of lower energy CRs at early times. This suppression is due to slower transport of lower energy CRs through the interstellar magnetic field environment and is more important at greater distances. In this work we revisit that modeling with revised calculations and update predicted effects in the 50 pc and 100 pc cases previously considered based on new results for SNCR flux. We also extend our modeling to SNe at 20 pc and 10 pc.

Comparing to past work, here we find in general lower SNCR flux, especially at lower primary energies and earlier times, with subsequently smaller impacts on ozone and sea-level radiation dose. Differences in ozone depletion are relatively small, but muon dose is significantly changed.

2 CALCULATION OF SUPERNOVA COSMIC RAY FLUX

Thomas et al. (2016) and Melott et al. (2017) describe methods and results of calculations of the flux at Earth of cosmic rays accelerated by supernovae at 100 pc and 50 pc, respectively. The methods applied, and results, depend on assumptions regarding the interstellar medium between Earth and the supernovae, most importantly the magnetic field environment. Since the cosmic rays (mostly protons) are charged particles, their path from the supernova to Earth is strongly affected by magnetic fields in the intervening medium, modulated by the particle energy (less effect for higher kinetic energy). In Thomas et al. (2016) three cases were considered. Cases A and B model propagation of cosmic rays from a supernova at 300 pc and 50 pc from a Galactic magnetic field line that passes through the solar system; Case B also assumes a low-energy cutoff of the flux, while Case A does not include such a cutoff. Case C considers a supernova at 100 pc and assumes the solar system exists in a region of interstellar medium already excavated by earlier supernova events, with the magnetic field environment dominated by a turbulent component of $0.1 \mu\text{Gauss}$. For that case, SNCR propagation can be modeled using the diffusion approximation. In Melott et al. (2017) two cases were considered. Case A assumes a GMF line runs directly from the SN through the solar system. Case B in Melott et al. (2017) is equivalent to Case C in Thomas et al. (2016), with only a turbulent magnetic field component, but for a SN placed at 50 pc instead of 100 pc.

In this work we use the magnetic field environment assumptions of Case C in Thomas et al. (2016) (Case B in Melott et al. (2017)). In those previous works an early-time, low-energy suppression was not applied, leading to an overestimate of the CR flux in certain cases. Here, we recompute the SNCR flux for SNe at 100 pc and 50 pc, and also perform new calculations for SNe at 20 pc and 10 pc.

We assume a purely turbulent magnetic field in the intervening space between the SNe and Earth, with field strength $0.1 \mu\text{G}$ (Avillez & Breitschwerdt 2005). The cosmic rays propagate isotropically and we compute the flux at Earth using a diffusive approximation

with $D(E) = D_0(E/E_0)^{1/3}$, $D_0 = 2 \times 10^{28} \text{ cm}^2 \text{ s}^{-1}$, and $E_0 = 1 \text{ GeV}$. Note that in Melott et al. (2017) the E_0 value is given as 10 GeV, which is a typographical error.

Given a source spectrum $Q(E) = Q_0 E^{-2.2} e^{-E/E_c}$ with $Q_0 = 3 \times 10^{52} \text{ protons GeV}^{-1}$ and $E_c = 1 \text{ PeV}$, the CR density at a distance r and time t after the initial release of CRs from the SN is given by $n(E, r, t) = \frac{Q(E)}{\pi^{3/2} r_{diff}^3} e^{-r^2/r_{diff}^2}$ with the effective diffusion distance $r_{diff}^2 = 4Dt$. The CR intensity is then given by $I = (c/4\pi)n$.

This approach assumes an instantaneous injection of CR by the SN. In reality, the injection is delayed until the remnant expands far enough to release the CR. While the release is therefore not actually instantaneous, we take this approximation as reasonable for our cases of interest.

The total CR energy we assume is $2.5 \times 10^{50} \text{ erg}$, consistent with estimates of typical Type II SNe (Kasen & Woosley 2009). As noted in Melott et al. (2017), this total energy is significantly higher than that used in Gehrels et al. (2003), the only other work reporting detailed modeling of effects on Earth's atmosphere from nearby SNe. In that work, the SNCR flux is approximated by a simple scale factor applied to the normal background Galactic cosmic ray flux, rather than explicit modeling of the flux.

As noted in Melott et al. (2017), the magnetic field environment in the intervening space is critical in determining the actual SNCR flux arriving at Earth. If a field line runs directly between the SNe and the solar system, the SNCR intensity will be much higher than modeled here. On the other hand, if the predominant field is perpendicular to the line of sight the SNCR flux will be strongly attenuated. We consider the diffusive transport case a middle-ground estimate between those two extremes.

2.1 SNCR flux results

In Figure 1 we show the calculated cosmic ray flux spectrum (times E^2 , so that the area under the curve is proportional to the total energy between limits) for all four distance

cases (100 pc, 50 pc, 20 pc, 10 pc), at several times. Times are measured from arrival of first photons from the SN. Also shown for reference in each case is the current Galactic cosmic ray (GCR) background.

Panel A in Figure 1 (the 100 pc case) compares to Case C in Figure 1 of Thomas et al. (2016), and Panel B in Figure 1 (the 50 pc case) compares to Case B in Melott et al. (2017). In those past works the flux was overestimated at energies below about 10^5 GeV and times earlier than about 3000 years (100 pc case) and energies below about 10^4 GeV and times earlier than about 1000 years (50 pc case). The main consequences of that difference, for our purposes, is a difference in calculated atmospheric ionization caused by the cosmic ray particles, and a difference in sea-level secondary muon flux. Panels C and D are new cases, with SNe at 20 pc and 10 pc.

3 ATMOSPHERIC IONIZATION AND CHEMISTRY MODELING

Atmospheric ionization by high-energy photons and cosmic rays has important effects on chemistry. Odd-nitrogen oxide compounds (NO_y , most importantly NO and NO_2) are produced, leading to destruction of stratospheric ozone and subsequent rain-out of HNO_3 (Thomas et al. 2005). Ionization by SNCRs in this work was computed using tables from Atri et al. (2010). The tables provide ionization rate (ions $\text{cm}^{-2} \text{s}^{-1}$) as a function of altitude for different primary proton energies from 300 MeV to 1 PeV, at 46 altitude bins, from the ground to 90 km. Here we used primary proton energies between 10 GeV and 1 PeV.

Effects on atmospheric chemistry by SNCR ionization were simulated using the NASA GSFC 2-D coupled chemistry-radiation-dynamics model. This model is an updated version of that used in Melott et al. (2017) and Thomas et al. (2016). In particular, the version used here includes feedbacks on temperatures fields due to changes in constituents such as ozone, which was not a feature of the previous version. This allows for more accurate simulation of the chemistry features as well as providing information about the associated temperature changes, which we were not able to

evaluate previously. In addition, the spatial resolution of the model has been increased to 4° latitude by 1 km altitude (from 10° latitude by 2 km altitude in the previous version), from the ground to about 92 km. A detailed description of this version of the model can be found in Fleming et al. (2011); see also (Fleming et al. 2015) and Airapetian et al. (2017). We run the model in a pre-industrial state, with anthropogenic compounds (such as CFCs) set to zero.

Ionization rates as a function of altitude for a particular case are generated by convolving the SNCR flux (essentially the number of incident protons at each energy) with the tables from Atri et al. (2010). The results are translated into production of NO_y , assuming 1.25 NO_y molecules per ion pair (Porter et al. 1976) at all altitude levels. The NO_y production rate is read in to the atmospheric model and the model run for 20 years until steady-state conditions were reached, simulating a steady-state flux of CRs. We then examine the concentrations of various constituents, especially O_3 , comparing a run with SNCR ionization input to a control run without that ionization source.

We use the updated version of the GSFC model with revised SNCR ionization profiles to revisit the atmospheric response in the 100 pc and 50 pc cases. In addition, we have performed new modeling of the 20 pc case.

We also sought to model the case of a 10 pc SN, roughly the distance commonly used as the standard “lethal” distance, based on Gehrels et al. (2003) which used a simple scaling up of the standard GCR ionization to simulate the effects of SNCRs. Here, we use the CR flux calculated as described above (shown in Figure 1). As may be seen in Figure 2 (panel D), the induced ionization for the 10 pc case is nearly 3 orders of magnitude above the background GCR ionization. When used in the newer GSFC model this very large ionization input produced non-physical results, due to numerical overflows. Therefore, in order to model the 10 pc case we have utilized the older, simpler version of the GSFC model (Thomas et al. 2005), which was able to handle the large ionization input and produced reasonable results, as compared to the other cases. We discuss results of all cases below.

3.1 Atmospheric ionization results

In Figure 2 we show atmospheric ionization rate profiles computed using the fluxes shown in Figure 1, for the same distance cases and times.

Comparing to previous work, here in the 100 pc case (Figure 2A) we find significantly smaller ionization than that in Thomas et al. (2016), due to the strong suppression at lower energies and earlier times, not included in the previous work. Recall that results presented here were generated using the assumptions of “Case C” in Thomas et al. (2016) and “Case B” in Melott et al. (2017) and all comparisons between this work and previous results are for that case. In Thomas et al. (2016), for the 100 pc case, ionization is maximized at the 500 year mark, with a factor of a few enhancement over the background GCR-induced ionization. Here we find that there is only a small enhancement over the GCR ionization and only at the lowest altitudes.

There is less of a difference in the 50 pc case (Figure 2B), comparing results here to those in Melott et al. (2017). In the previous work a maximum enhancement over background of about 50 times was seen, while here the increase is closer to 10 times. However, the timing of that increase changes from the 100-300 year range in the previous work to the 300-1000 year range in this work. Essentially, the time of maximum impact is shifted later due to the early suppression included here, which was neglected in the previous work.

In Figure 2 panels C and D we present ionization results for the 20 pc and 10 pc cases, respectively. As may be expected, the ionization rates are higher in these cases and the time variation is simpler due to the less pronounced (or absent) early suppression. Maximum enhancement over background in the 20 pc case is around 200 times and in the 10 pc case around 1000 times.

3.2 Atmospheric chemistry results

In order to evaluate the impact on O₃, we computed the percent difference in column density values between the SNCR cases and a control run of the model with no additional ionization input. In Figure 3 we show the globally averaged percent difference in column density of O₃ for the 20 pc, 50 pc, and 100 pc cases at the times of maximum ionization.

For the 100 pc case the maximum ionization occurs at the 3000 year mark. Using those ionization results in the atmospheric chemistry model we find globally averaged depletion around 2%. This is slightly smaller than that reported in Thomas et al. (2016), which is expected due to the lower ionization in this work compared to that past work.

For the 50 pc case the maximum ionization occurs at the 1000 year mark. In this case we find globally averaged depletion around 17%. This is somewhat smaller than the 25% reported in Melott et al. (2017), which is again attributable to the smaller ionization values in this work compared to that past work.

For the 20 pc case (new to this work) the maximum ionization occurs at the earliest modeled time (100 years). The resulting globally averaged depletion is about 62%. In Figure 4 we show the percent difference (compared to control) in O₃ column density as a function of latitude and time for this case. Notice that there is significant depletion, over 30%, at all latitudes, up to 87% in the polar regions.

As discussed above, for the 10 pc case we have used the simpler GSFC model version (without temperature feedback and lower spatial resolution) since the newer, more complex model is not able to simulate conditions under the very high ionization rates for this case. Using that simpler model we find globally averaged depletion only slightly higher than the 20 pc case. This is not surprising given that O₃ depletion scales roughly with energy input as a power law with index ~ 0.3 (Thomas et al. 2005), reflecting the fact that depletion “saturates” as it approaches 100%. In Figure 5 we show the percent difference (compared to control) in O₃ column density as a function of latitude and time for this case. Note that in this case there are isolated areas in the polar regions where

O₃ column density is briefly *higher* than the control case. This effect was explored for the case of a gamma-ray burst (GRB) (Thomas et al. 2005) and is the result of extremely high production of nitrogen oxides which, through photochemical processes, result in short-term *production* of O₃ at the start of South Polar spring.

Finally, we investigated possible effects on atmospheric chemistry under increased lightning rates, as suggested in Melott & Thomas (2019). The GSFC model includes lightning as an input to nitrogen oxide production, which near Earth's surface participates in chemistry that *increases* O₃ concentration. We modified the model to scale up lightning rates based on the enhancement of ionization in SNCR cases over the background GCR ionization. Given that little is known about the magnitude of change in lightning for a given change in ionization, we used a simple linear scaling. Past work examined effects of increased surface-level O₃ in the case of a GRB (Thomas & Goracke 2016), finding that the concentration was nearly doubled for a particular case, but the increase was not large enough to cause biological damage. In the 20 pc case considered here we find a maximum increase over control of about 2.5%. Since this is much smaller than the GRB case we will not consider it further.

4 SEA-LEVEL MUON FLUX

Following Thomas et al. (2016) and Melott et al. (2017) we calculated sea-level muon flux by convolving our calculated SNCR spectra with the table of Atri & Melott (2011) and then used the result to compute radiation dose. As discussed in Melott et al. (2017), radiation doses for muons have not been measured for the energies relevant to this work, so we have used the energy deposition in water and a radiation-weighting factor of 1 (the same as for electrons).

In Figure 6 we show results of the muon flux calculations. Comparing our results for the 50 pc diffusive case considered here (Figure 6 panel A) to the equivalent 50 pc case (Case B) in Melott et al. (2017), the maximum flux occurs at the 1000 year (instead of 100 year) mark and the maximum is roughly an order of magnitude smaller than seen in the previous work. This is due to the lower energy CR suppression included here that

was previously neglected. In fact, the Melott et al. (2017) results more closely match our calculations for the 20 pc case (Figure 6 panel B).

In Table 1 we present the calculated annual muon radiation dose, in mSv, for our 20 pc and 50 pc cases, and those from Case B in Melott et al. (2017) for comparison.

Unlike the O₃ depletion results discussed above, where this updated study finds roughly similar results to past work, in the case of muon dose there is a significant difference, with previous work over-estimating the dose in the 50 pc case by roughly an order of magnitude. This difference can be attributed to the strong suppression previously neglected in Melott et al. (2017) at the energies relevant for muon flux (at the early time points).

5 DISCUSSION AND CONCLUSIONS

The goals of this work were two-fold. First, to re-evaluate recent work (Melott et al. 2017; Thomas et al. 2016) on nearby supernovae at 100 pc and 50 pc in the diffusive transport cosmic ray case, since that work neglected an early time suppression at lower cosmic ray energies. Inclusion of this suppression leads to lower overall CR flux at early times, lower atmospheric ionization, smaller resulting ozone depletion, and lower sea-level muon radiation dose. Differences are most pronounced for the 100 pc case with only a small enhancement in low altitude ionization and small globally averaged decrease in column O₃. We can conclude that, for the specific parameters considered in this study, 100 pc is too far to result in noticeable terrestrial effects.

For the 50 pc case, enhancement in low altitude ionization and globally averaged decrease in column O₃ are smaller than those reported in Melott et al. (2017), but the differences are relatively small and do not significantly change the conclusions of that work or subsequent work based on those results (Melott et al. 2020, 2019; Melott & Thomas 2019; Thomas 2018; Thomas & Ratterman 2020). We expect that a 50 pc SN would have noticeable terrestrial effects, but perhaps not dramatic enough to be obvious in the fossil record.

Our second goal was to perform new modeling for SNe at 20 pc and 10 pc. While geochemical evidence supports the occurrence of at least one SN within the 50-100 pc range about 2.6 Mya, there is no direct evidence of SNe closer than 50 pc. However, it is likely that there has been at least 1-2 SNe at a 10-20 pc range within the last 500 Mya (Melott & Thomas 2011).

We find that already at 20 pc the SNCRs cause major global O₃ depletion, which would last on the order of centuries to millennia. The maximum O₃ depletion is limited by essentially running out of O₃ to destroy, coupled with O₃ production mechanisms that offset depletion and continue regardless of ionization input, so that distances closer than 20 pc result in only marginally greater depletion.

Regarding the sea-level muons, we found that Melott et al. (2017) dramatically overestimated the radiation dose at 50 pc. In fact, those past values are more comparable to our results for a 20 pc SN. Based on these results, it appears unlikely that muon radiation is a significant threat to the biosphere for SN beyond at least 20 pc. This finding implies that results reported in Melott et al. (2019) are likely not accurate for a 50 pc SN, but would apply for a SN at 20 pc.

It should be noted that the present study includes only the effects of cosmic rays associated with the supernova explosions. These changes occur centuries and longer after any electromagnetic emission is received. Any high energy light (ie. X-rays) would also have an effect on the atmosphere, but that impact will only persist for a decade or so (Gehrels et al. 2003; Thomas et al. 2005), while the cosmic ray impact will persist for 100s to 1000s of years.

Perhaps most importantly, this study indicates that the “lethal” SN distance should be closer to 20 pc rather than the typically quoted 8-10 pc. This again is based only on effects due to CRs from the SN. With a larger distance, such SN events become more

common and may be associated with more instances of extinctions, and possibly climate change periods, during the Phanerozoic.

The 20 pc distance is particularly significant since it has been suggested (Fields et al. 2020) that extinctions at the end of the Devonian period may have been triggered by supernova explosions at roughly 20 pc. In that work it was assumed that 20 pc was somewhat beyond the “lethal” distance necessary to initiate a mass extinction. Our results here indicate that in fact 20 pc may well be a mass extinction-inducing distance. The less severe biodiversity crisis at the end-Devonian may indicate a larger distance of any associated supernovae, perhaps as far as 50 pc. Importantly, a larger distance increases the likelihood of a supernova event, thereby potentially strengthening the argument presented in Fields et al. (2020).

In addition to the long-term CR effects studied here, recent work (Brunton et al. 2022) indicates that effects of SN X-ray emission may be as important as the CR impacts, though much shorter-lived, even out to 50 pc. Supernovae as far as 50 pc may therefore present both a short- and long-lived lethal threat for Earth and any Earth-like planet with similar atmospheric conditions. This greatly increases the likelihood that at least one and perhaps several extinctions in the fossil record may be associated with nearby supernovae.

Of course, it should be noted that determining the “lethality” of an astrophysical ionizing radiation event based on O₃ depletion level is highly uncertain and much more work is needed to establish the connection between specific O₃ depletion level and magnitude of impact on the biosphere.

ACKNOWLEDGEMENTS

The authors thank M. Kachelrieß and A. Melott for helpful discussions regarding updated SNCR modeling and this manuscript.

DATA AVAILABILITY

The data underlying this article are freely available at zenodo.org

REFERENCES

- Airapetian, V. S., Jackman, C. H., Mlynczak, M., Danchi, W., & Hunt, L. 2017, *Sci Rep*, 7, 14141
- Atri, D., & Melott, A. L. 2011, *Radiat Phys Chem*, 80, 701
- Atri, D., Melott, A. L., & Thomas, B. C. 2010, *J Cosmol Astropart Phys*, 2010, 008
- Avillez, M. A. de, & Breitschwerdt, D. 2005, *Astron Astrophys*, 436, 585
- Binns, W. R., Israel, M. H., Christian, E. R., et al. 2016, *Science*, 352, 677
- Breitschwerdt, D., Feige, J., Schulreich, M. M., et al. 2016, *Nature*, 532, 73
- Brunton, I. R., O'Mahoney, C., Fields, B. D., Melott, A. L., & Thomas, B. C. 2022, <http://arxiv.org/abs/2210.11622>
- Fields, B. D., Melott, A. L., Ellis, J., et al. 2020, *Proc Natl Acad Sci*, 117, 21008
- Fimiani, L., Cook, D. L., Faestermann, T., et al. 2016, *Phys Rev Lett*, 116, 151104
- Fleming, E. L., George, C., Heard, D. E., et al. 2015, *J Geophys Res Atmospheres*, 120, 5267
- Fleming, E. L., Jackman, C. H., Stolarski, R. S., & Douglass, A. R. 2011, *Atmospheric Chem Phys*, 11, 8515
- Fry, B. J., Fields, B. D., & Ellis, J. R. 2016, *Astrophys J*, 827, 48
- Gehrels, N., Laird, C. M., Jackman, C. H., et al. 2003, *Astrophys J*, 585, 1169
- Kasen, D., & Woosley, S. E. 2009, *Astrophys J*, 703, 2205
- Knie, K., Korschinek, G., Faestermann, T., et al. 2004, *Phys Rev Lett*, 93, 171103
- Ludwig, P., Bishop, S., Egli, R., et al. 2016, *Proc Natl Acad Sci*, 113, 9232
- Melott, A. L., Marinho, F., & Paulucci, L. 2019, *Astrobiology*, 19, 825
- Melott, A. L., & Thomas, B. C. 2011, *Astrobiology*, 11, 343
- Melott, A. L., & Thomas, B. C. 2019, *J Geol*, 127, 475
- Melott, A. L., Thomas, B. C., & Fields, B. D. 2020, *Int J Astrobiol*, 19, 349
- Melott, A. L., Thomas, B. C., Kachelrieß, M., Semikoz, D. V., & Overholt, A. C. 2017, *Astrophys J*, 840, 105
- Porter, H. S., Jackman, C. H., & Green, A. E. S. 1976, *J Chem Phys*, 65, 154
- Thomas, B. C. 2018, *Astrobiology*, 18, 481
- Thomas, B. C., Engler, E. E., Kachelrieß, M., et al. 2016, *Astrophys J Lett*, 826, L3
- Thomas, B. C., & Goracke, B. D. 2016, *Astrobiology*, 16, 1
- Thomas, B. C., Melott, A. L., Jackman, C. H., et al. 2005, *Astrophys J*, 634, 509
- Thomas, B. C., & Ratterman, C. L. 2020, *Phys Rev Res*, 2, 043076
- Wallner, A., Feige, J., Fifield, L. K., et al. 2020, *Proc Natl Acad Sci*, 117, 21873
- Wallner, A., Feige, J., Kinoshita, N., et al. 2016, *Nature*, 532, 69

FIGURES

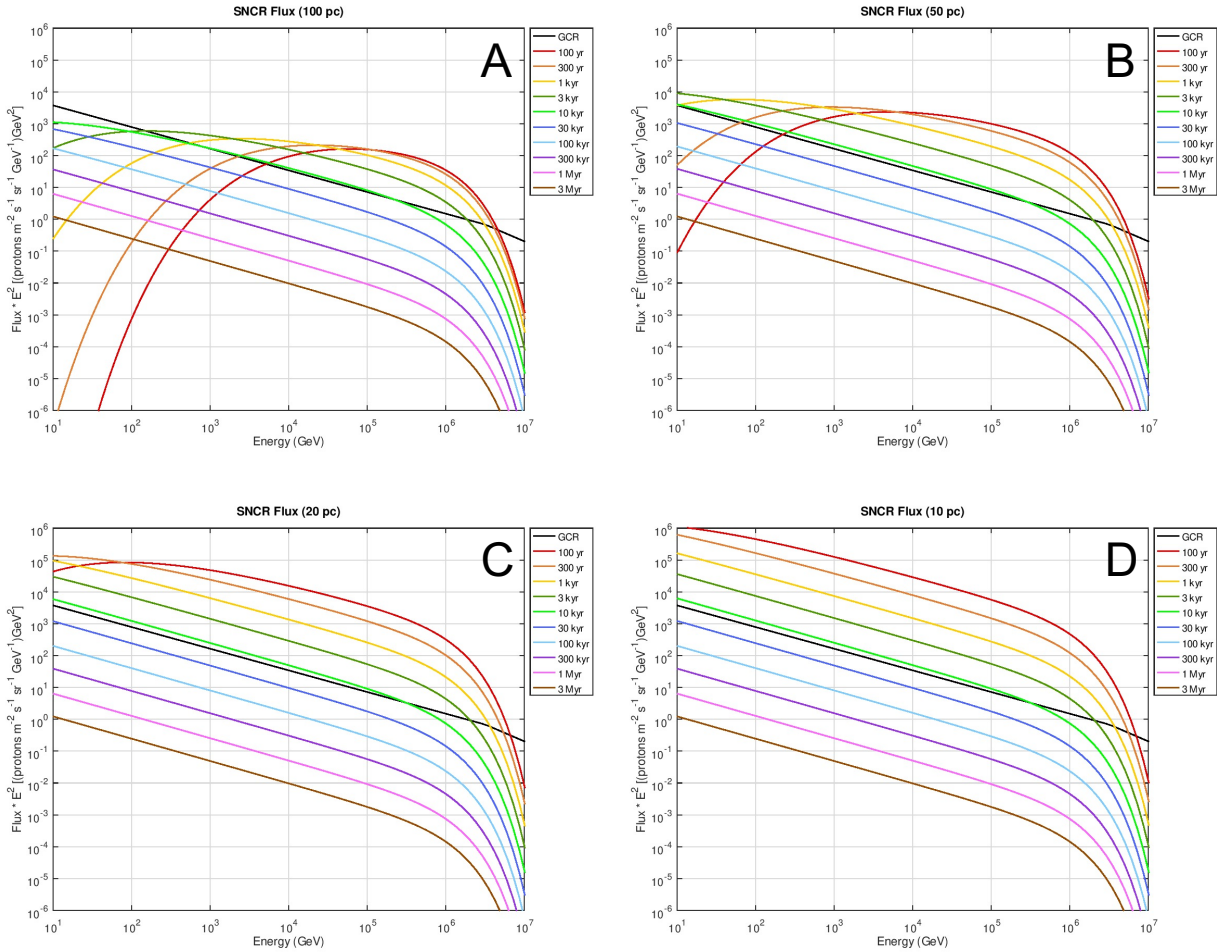


Figure 1 – Cosmic-ray flux spectrum (times E^2) for SN at 100 pc (A), 50 pc (B), 20 pc (C), and 10 pc (D), at times from 100 years to 3 million years after arrival of first photons from the SN. The present-day Galactic cosmic-ray background flux (GCR) spectrum is shown in each panel (black line) for reference.

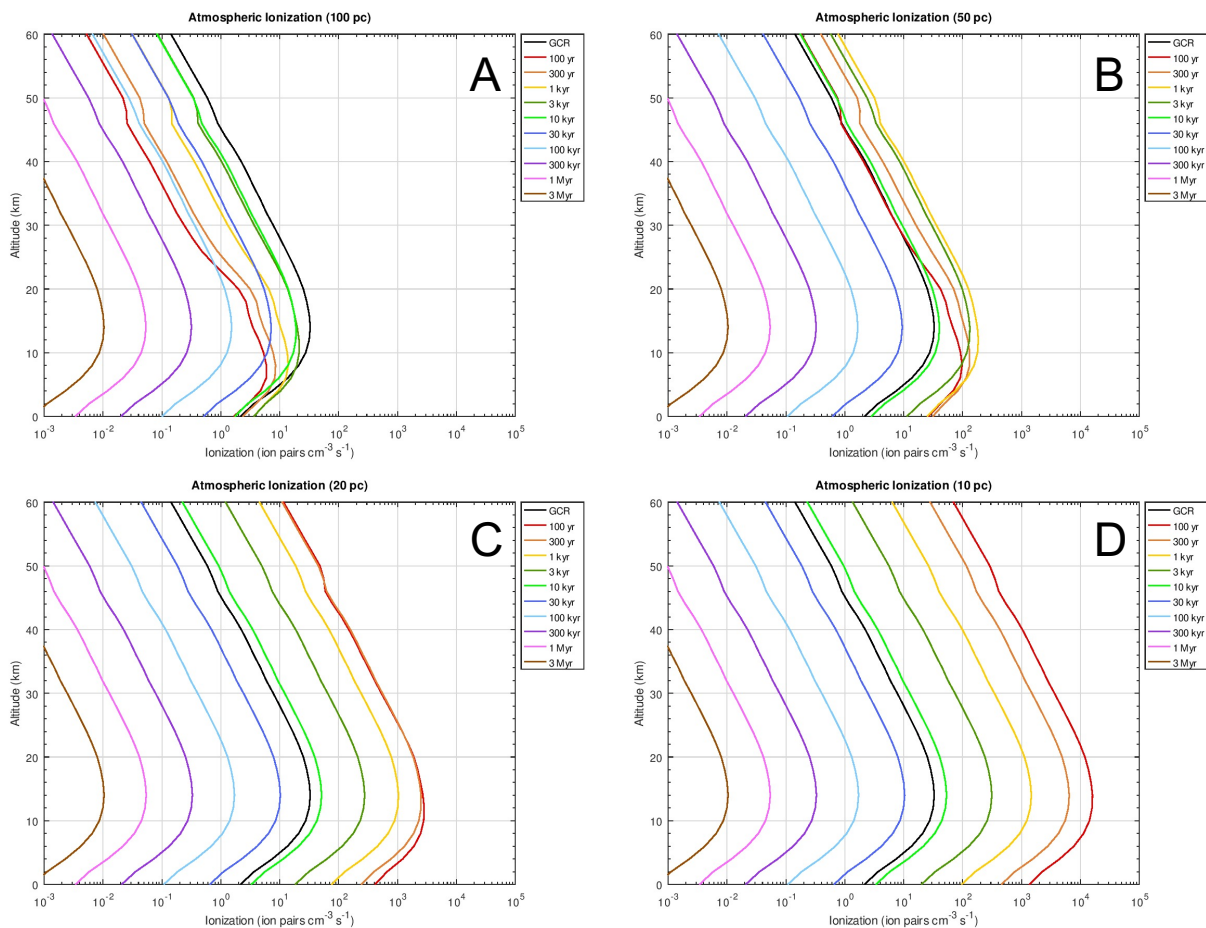


Figure 2 – Atmospheric ionization rate profiles for ionization caused by CRs from SN at 100 pc (A), 50 pc (B), 20 pc (C), and 10 pc (D), at times from 100 years to 3 million years after arrival of first photons from the SN. The present-day ionization profile caused by GCRs is shown in each panel (black line) for reference.

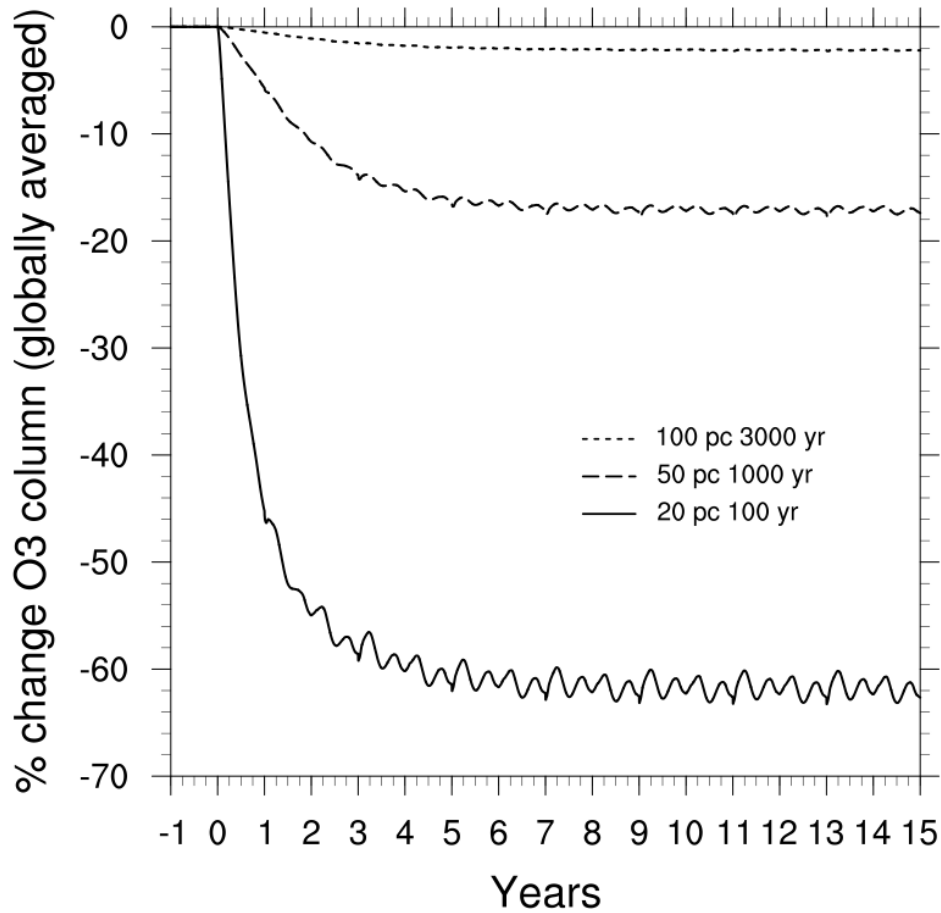


Figure 3 - Globally averaged change (per cent difference vs control) in atmospheric O₃ column density, assuming steady-state irradiation after time 0 for SN at 100 pc (dotted line), 50 pc (dashed line), 20 pc (solid line). Times (3000 yr, 1000 yr, 100 yr) correspond to those in Figures 1 and 2, and represent the epoch of maximum O₃ depletion for each case.

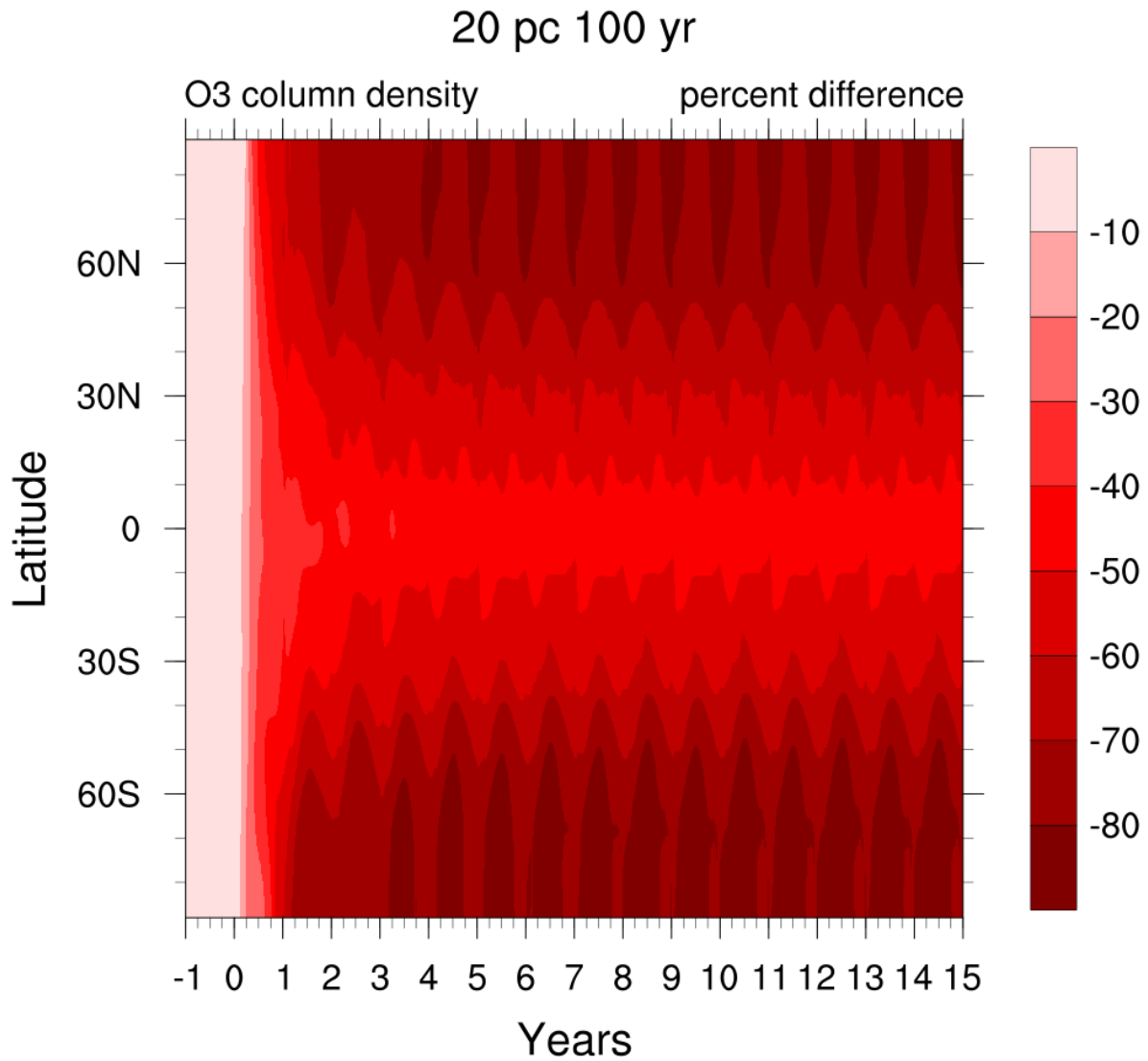


Figure 4 - Per cent difference (versus control) in O₃ column density, as a function of latitude and time for the 20 pc SN case at 100 years after arrival of photons, assuming steady-state irradiation after time 0.

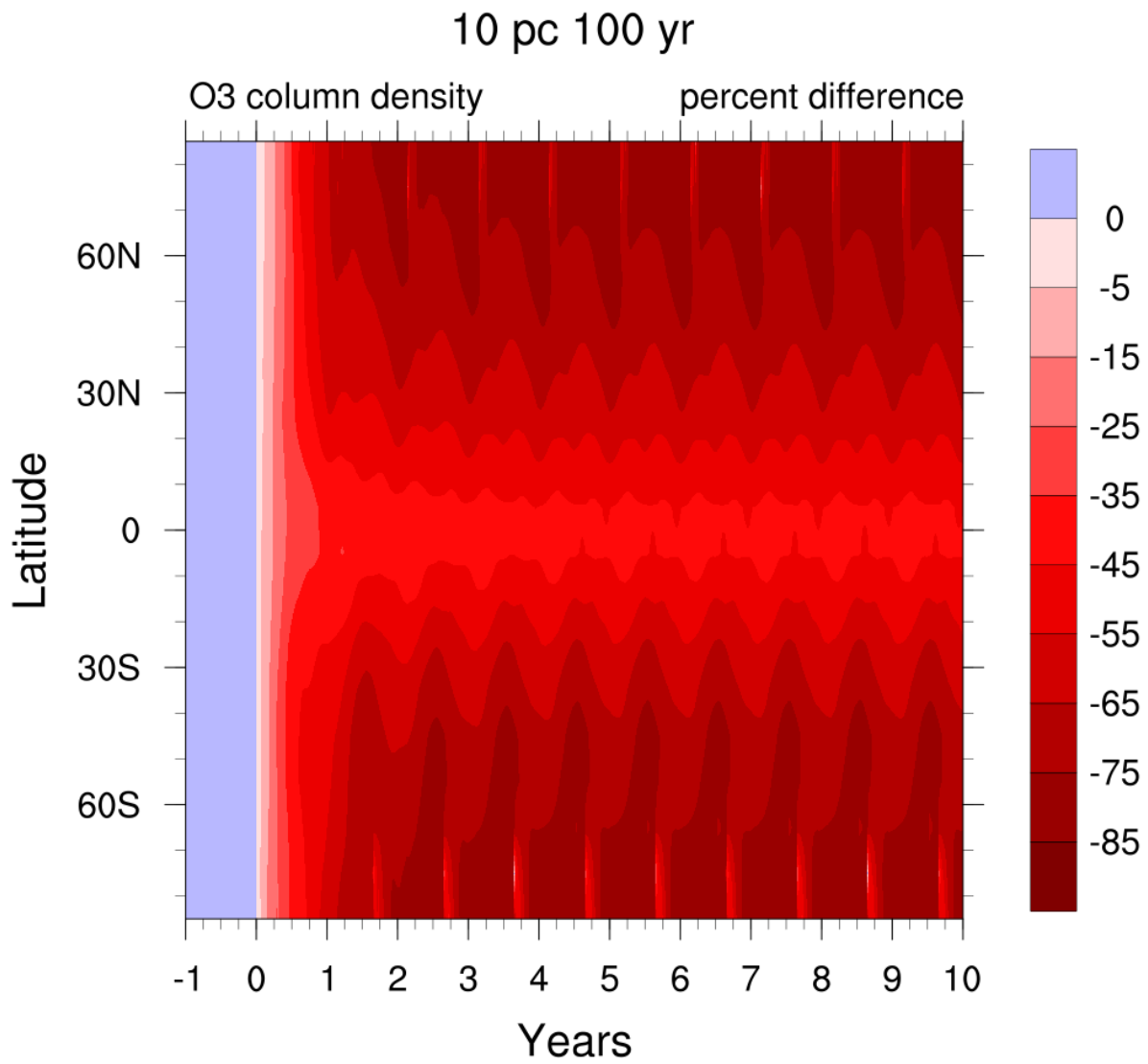


Figure 5 - Per cent difference (versus control) in O₃ column density, as a function of latitude and time for the 10 pc SN case at 100 years after arrival of photons, assuming steady-state irradiation after time 0.

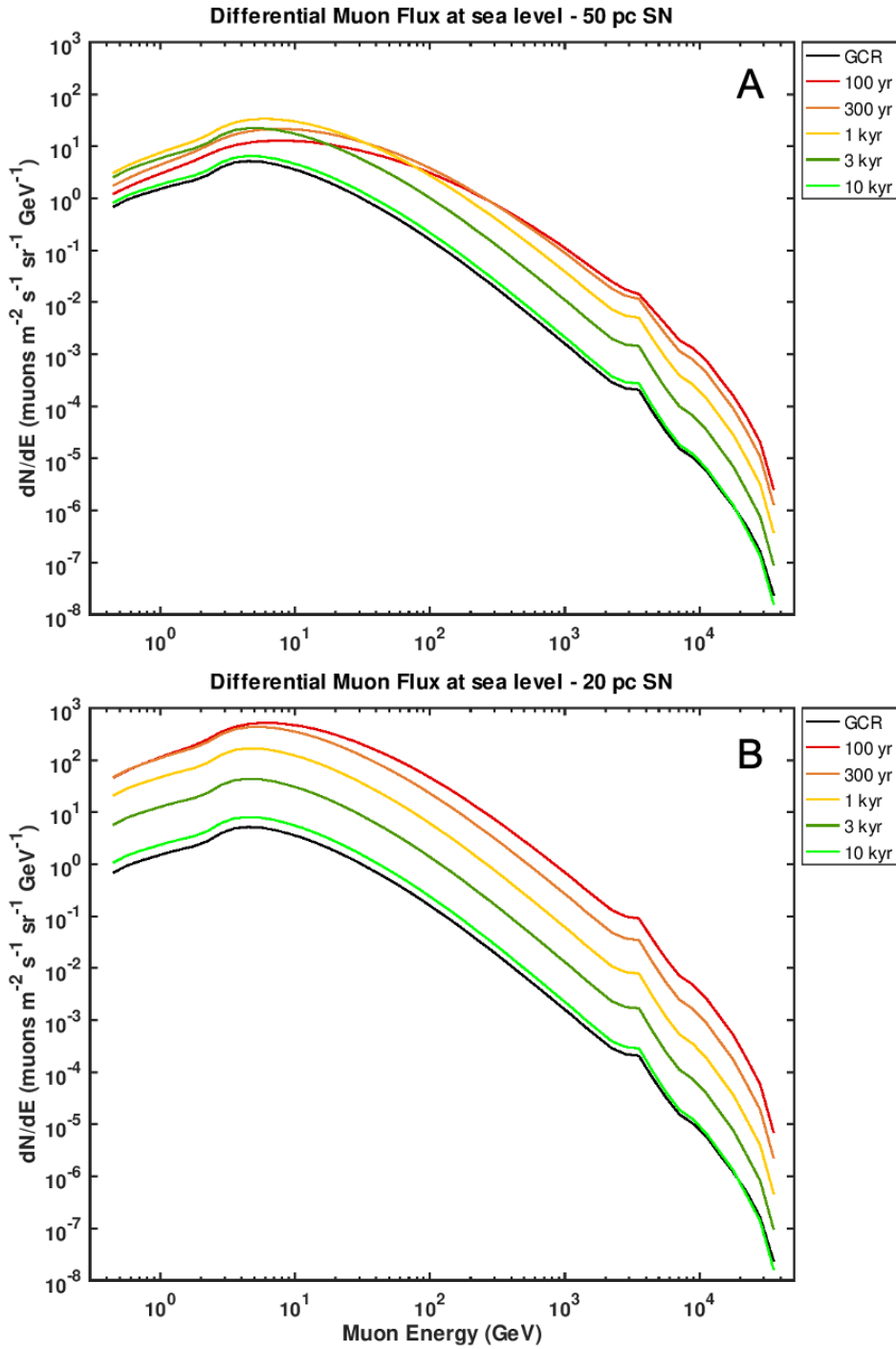


Figure 6 - Differential muon spectrum at sea level for SN at 50 pc (A) and 20 pc (B) at several times (corresponding to those in Figure 1). The black line represents the typical present spectrum, primarily as a result of showers initiated by Galactic cosmic-rays (GCR).

TABLES

Table 1: Annual Ground Level Muon Radiation Dose, in Units of mSv, for two SN Cases in this work and for Case B in Melott et al. (2017)

Time	20 pc	50 pc	2017 50 pc Case B
100 years	36.9	2.66	31.5
300 years	20.9	2.87	21.1
1 kyr	6.28	2.22	8.36
3 kyr	1.49	0.966	2.61
10 kyr	0.266	0.23	0.587

Note: For comparison, the present-day average annual dose on the ground due to muons is about 0.20 mSv.